Theoretical study of thermoelectric properties of MoS_2*

Guo Huai-Hong(郭怀红), Yang Teng(杨 腾)†, Tao Peng(陶 鹏), and Zhang Zhi-Dong(张志东)

Shenyang National Laboratory for Materials Science, Institute of Metal Research and International Center for Materials Physics, Chinese Academy of Sciences, Shenyang 110016, *China*

(Received 12 August 2013; revised manuscript received 26 September 2013; published 12 November 2013)

We systematically studied the thermoelectric properties of MoS_2 with doping based on the Boltzmann transport theory and first-principles calculations. We obtained an optimal doping region (around 10^{19} cm^{-3}) for thermoelectric properties along in-plane and cross-plane directions. MoS_2 in the optimal doping region has a vanishingly small anisotropy of thermopower possibly due to the decoupling of in-plane and cross-plane conduction channels, but big anisotropies of electrical conductivity σ and electronic thermal conductivity κ_e arising from the anisotropic electronic scattering time. The κ_e is comparable to the lattice counterpart κ_l in the plane, while κ_l dominates over κ_e across the plane. The figure of merit ZT can reach 0.1 at around 700 K with in-plane direction preferred by doping.

Keywords: MoS_2, thermoelectric properties, doping, anisotropy

PACS: 72.20.Pa, 72.80.Ga, 31.15.A– **DOI:** 10.1088/1674-1056/23/1/017201

1. Introduction

Transition-metal dichalcogenide MoS_2 is one prototype material in the chalcogenide family that has attracted tremendous attention in the last few decades due to its distinctive electronic, mechanical, catalytic and tribological properties.[1–10] Recent research on its optical properties[11] and lattice dynamics[12,13] has aroused renewed interest. Especially, the lowest thermal conductivity has been obtained experimentally in an MoS_2-related structure,[14,15] which together with an unusually large thermopower[16–18] found in MoS_2, may render it a potential candidate for thermoelectrics. A possible drawback is the poor electrical conductivity of MoS_2. As a matter of fact, an external stress has been lately proposed to improve the electrical conductivity.[19] A pressure-induced semiconductor–metal transition is found to be advantageous for the inter-plane thermoelectric transport. However, a pressure as high as a few tens of GPa would entail a practical problem for use.

Electronic doping has been a useful means for improving the thermoelectric properties of semiconductors.[20–24] Nevertheless, available experimental data concerning the thermoelectric transport properties of doped MoS_2 are quite scarce, fragmentary in the literature and far from optimization. It remains a big challenge and costly to experimentally dope in a wide region to find an optimum figure of merit ZT. The most significant experimental work was performed by Mansfield and Salam[17] and Thakurta *et al.*,[16] who studied the temperature dependence of the electrical transport properties, including thermopower and electrical conductivity in three samples with low dopings; however, they failed to investigate the thermal-related properties. Kim *et al.*[15] merely worked on the thermal conductivity κ. Based on those incomplete experimental data, it is not possible to evaluate the thermoelectric efficiency nor to find a proper doping region to optimize it.

In this paper, we study theoretically the thermoelectric transport properties of MoS_2 to find an optimal doping for improving its thermoelectric conversion efficiency. We have so far found the following results. (i) Thermopower more than 200 μV/K is attainable over a wide range of dopings, agreeing with the experimental results. A directional anisotropy between in-plane and cross-plane thermopowers exists at low doping levels but vanishes above 10^{17} cm^{-3}, which probably arises from the decoupling of in-plane and cross-plane conduction channels. (ii) An anisotropic electronic scattering time is found to exist between in-plane and cross-plane directions, which accounts for two orders of magnitude difference between electrical conductivities σ_{xx} and σ_{zz} and also gives rise to an anisotropy between electronic thermal conductivities κ_e^{xx} and κ_e^{zz}. (iii) In the optimal doping region, electronic thermal conductivity κ_e is not negligible compared to lattice thermal conductivity κ_l in the plane, while κ_l dominates over κ_e across the plane. (iv) A carrier density around 10^{19} cm^{-3} is sufficient for optimal thermoelectric performance, the figure of merit coefficient reaches 0.1 at 700 K within the plane and a preference for in-plane over cross-plane direction by doping is demonstrated.

2. Methods

The band structure of MoS_2 is calculated by using the general potential linearized augmented plane-wave (LAPW)

*Project supported by the National Natural Science Foundation of China (Grant Nos. 11004201 and 51331006), the National Basic Research Program of China (Grant No. 2012CB933103), and the IMR SYNL-Young Merit Scholars and T. S. Kê Research Grant, China.

†Corresponding author. E-mail: yangteng@imr.ac.cn

© 2014 Chinese Physical Society and IOP Publishing Ltd

method as implemented in the WIEN2K package.[25] The electronic exchange–correlation is described within the generalized gradient approximation (GGA) of Perdew–Burke–Ernzerhof (PBE) flavor[26] and the Engel–Vosko GGA (EV-GGA) formalism[27] is used to improve the band gap calculations. We use 5000 k points in the full Brillouin zone (BZ) to achieve a total energy convergence better than 1 meV/atom. MoS_2 has P_{63}/mmc space group symmetry and consists of a hexagonal plane of molybdenum atoms sandwiched by two hexagonal planes of sulfur atoms. The unit cell contains two alternating and weakly van der Waals bonded layers with an AB stacking along the c axis. The experimental lattice parameters[28] ($a = 3.16$ Å, $c = 12.295$ Å) are used here.

The transport properties can be obtained from the conductivity distributions

$$\sigma_{\alpha\beta}(T;\mu) = \frac{1}{\Omega}\int \sigma_{\alpha\beta}(\varepsilon)\left[-\frac{\partial f_\mu(T;\mu)}{\partial\varepsilon}\right]\mathrm{d}\varepsilon, \quad (1)$$

$$\kappa_{\alpha\beta}(T;\mu) = \frac{1}{e^2T\Omega}\int \sigma_{\alpha\beta}(\varepsilon)(\varepsilon-\mu)^2\left[-\frac{\partial f_\mu(T;\mu)}{\partial\varepsilon}\right]\mathrm{d}\varepsilon, \quad (2)$$

$$S_{\alpha\beta}(T;\mu) = \frac{(\sigma^{-1})_{\gamma\alpha}}{eT\Omega}\int \sigma_{\gamma\beta}(\varepsilon)(\varepsilon-\mu)\left[-\frac{\partial f_\mu(T;\mu)}{\partial\varepsilon}\right]\mathrm{d}\varepsilon, \quad (3)$$

where $\sigma_{\alpha\beta}$, $\kappa_{\alpha\beta}$ and $S_{\alpha\beta}$ are the electrical conductivity, electronic thermal conductivity and thermopower, respectively. The energy projected conductivity tensor $\sigma_{\alpha\beta}(\varepsilon)$ is defined as[29]

$$\sigma_{\alpha\beta}(\varepsilon) = \frac{1}{N}\sum_{i,k}\sigma_{\alpha\beta}(i,k)\frac{\delta(\varepsilon-\varepsilon_{i,k})}{d\varepsilon}, \quad (4)$$

with

$$\sigma_{\alpha\beta}(i,k) = e^2\tau_{i,k}v_\alpha(i,k)v_\beta(i,k), \quad v_\alpha(i,k) = \frac{1}{\hbar}\frac{\partial\varepsilon_{i,k}}{\partial k_\alpha}, \quad (5)$$

where τ is the electronic relaxation time; group velocity v_α can be calculated from band structure $\varepsilon_{i,k}$.

We calculate the transport properties based on the Boltzmann transport theory applied to the band structure, which is different from the empirical method used by Wu *et al.*[21] and the quantum ballistic method adopted by Hu *et al.*[30] In the following part, we discuss the dependences of transport functions including thermopower S, electrical conductivity σ, power factor (FP) and ultimately figure of merit coefficient ZT on the temperature and doping level along two perpendicular directions. The electron scattering time is assumed to be independent of energy due to its good description of $S(T)$ in a number of thermoelectric materials.[6,31,32] In this sense, no adjustable parameters are needed to calculate these transport functions. The integration is done within the BOLTZTRAP transport code.[29] A very dense mesh with up to 18000 k points in the BZ is used.

3. Results and discussion

In Fig. 1, we present our calculated EV-GGA band structure and density of states of MoS_2. The in-plane and cross-plane cases are considered separately in Figs. 1(a) and 1(b). In Fig. 1(a), an indirect gap of 1.04 eV is obtained between the top of the valence band at Γ and the bottom of the conduction band at one k point between K and Γ. A similar band structure calculated with the standard PBE-GGA formalism gives an indirect gap of 0.84 eV, which agrees with the reported value.[33] Compared with $\Delta_i \sim 1.20$ eV from experiment,[34] it is clear that the EV-GGA does improve the band gap calculation upon the PBE-GGA. The structural anisotropy induces an anisotropy between in-plane and cross-plane band gaps. The calculated cross-plane gap is found to be 2.20 eV.

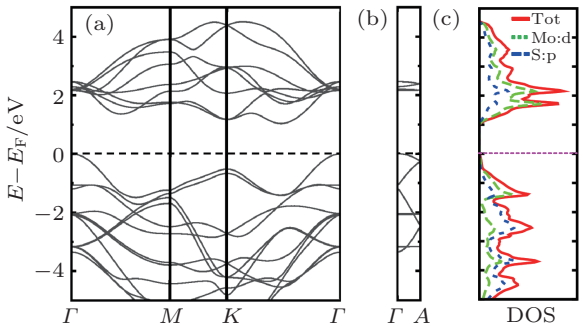


Fig. 1. (color online) EV-GGA electronic band structure of MoS_2 along high-symmetry lines (a) Γ–M–K–Γ in plane and (b) Γ–A across plane in the hexagonal Brillouin zone. The valence-band edge is set as zero and marked with a dashed line. In panel (c), the electron density of states at the conduction band edge is comparatively higher than that at the valence band edge.

Besides the band gap anisotropy, a strong asymmetric feature between the valence and the conduction bands implies that the thermoelectric properties of n-type (electron-doping) MoS_2 would be very different from those of p-type (hole doping). The heavy and doubly degenerate bands near the conduction-band minimum suggest that the n-type MoS_2 would have a better thermoelectric performance. In Fig. 1(c), the total density of states (DOS) also shows this possibility, the DOS very close to the conduction band edge is comparatively higher than that near the valence band edge. Considering more experimental data have been found for the p-type in the literature,[16–18] we focus on hole-doped MoS_2 in this study.

In-plane and cross-plane thermopowers are firstly studied. We compare our calculated S with the experimental data from Mansfield and Salam[17] in Figs. 2(a) and 2(b). Samples in their experiment were p-type from nature with a hole carrier concentration as low as 10^{15}–10^{17} cm^{-3}. A very good agreement is obtained. Both our calculation and the available experimental data show an in-plane thermopower S higher than 400 μV/K and S decreases with increasing temperature, as shown in Fig. 2(a). Then we extend our discussion to

high doping of 10^{17}–10^{20} cm^{-3} (corresponding to hole carrier concentration of $p = 10^{-5}$–10^{-2} holes per unit cell in our case) where the thermoelectric properties are expected to be optimized, as predicted from theory[34] and observed experimentally in many materials.[35–37] It also applies in MoS_2, as we will show later. From Fig. 2(b), the thermopower in the high doping region, though decreasing with increasing doping level, takes a value of at least 200 μV/K and increases with increasing temperature. To see a possible anisotropy usually expected in layered structures,[38–40] we then show the ratio of S_{zz} over S_{xx} in Fig. 2(c). A relatively high anisotropy of thermopower below 10^{17} cm^{-3} is observed; however, it vanishes as the doping goes above 10^{17} cm^{-3} where both S_{xx} and S_{zz} having the same magnitude show a similar dependence on the hole doping level and temperature, which is different from the layered conductive thermoelectric oxides.[38–40] To understand the disappearance of the thermopower anisotropy based on the Mott formula[34] ($S \sim \partial \ln(n\mu)/\partial E$, where n and μ are respectively the carrier density and the mobility), we consider separately the two-dimensional in-plane channel and the one-dimensional cross-plane one due to the decoupling of the two perpendicular channels, which was also observed in other layered anisotropic structures.[38,39] The band near the valence band maximum (VBM), as seen from Figs. 1(a) and 1(b), is approximately parabolic, suggesting that the effective mass (or mobility μ) is almost independent of doping (or energy). In the meantime, the in-plane electron density of states is constant, while a van-Hove singularity is anticipated for the cross-plane DOS near the VBM, explaining why S_{zz} is much smaller than S_{xx} in the low doping region. However, with a moderate doping, the cross-plane Fermi energy will be shifted away from the big DOS value of singularity. We therefore expect that a similar dependence of the carrier density on energy for both directions will suppress the anisotropy between them. Finally, to confirm that n-type MoS_2 may have a larger thermopower, we briefly compare n-type in Fig. 2(d) with p-type in Fig. 2(b). As expected, thermopowers of n-type MoS_2 bigger than those of p-type are found.

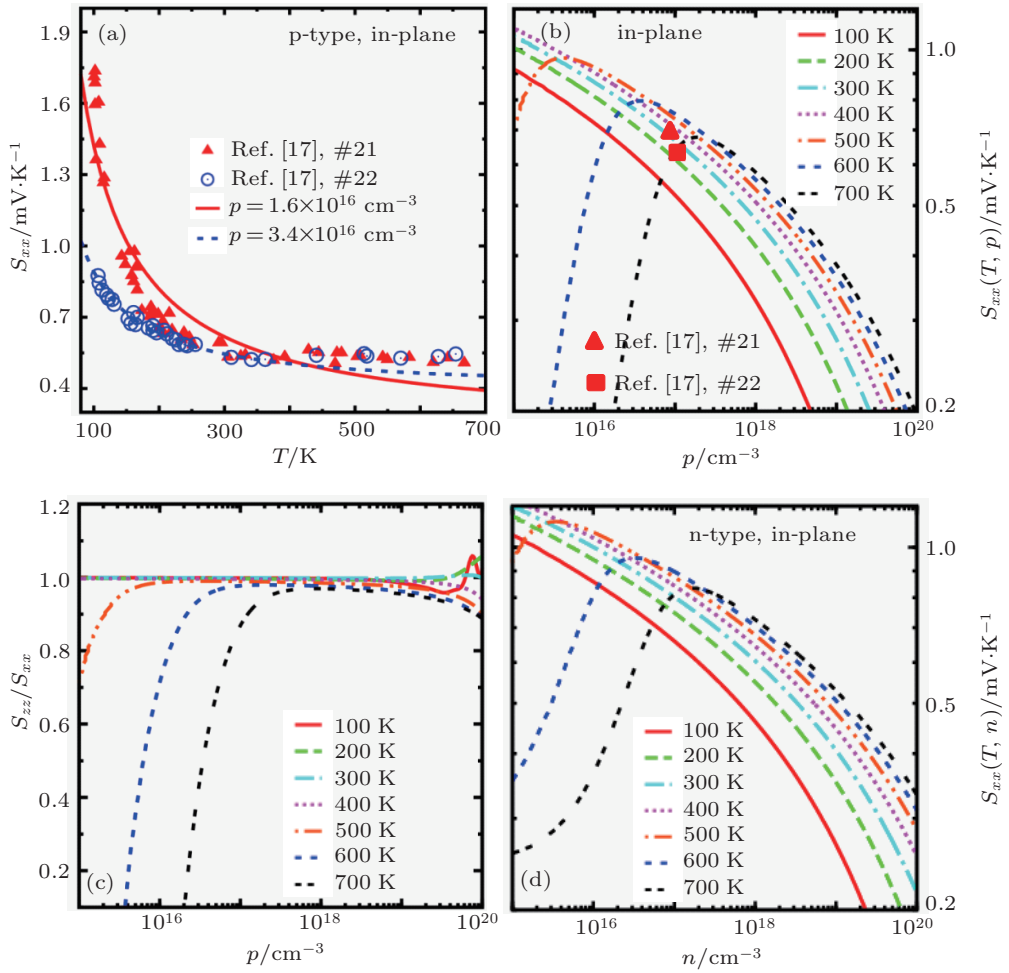


Fig. 2. (color online) (a) Temperature dependence of calculated in-plane thermopower S_{xx} of MoS_2, compared with the experimental data by Mansfield and Salam[17] at two hole-doping levels $p = 1.6 \times 10^{16}$ (filled triangle) and 3.4×10^{16} (empty circle) holes per cm^3. Doping level dependences of (b) in-plane thermopower $S_{xx}(p,T)$, (c) ratio of cross-plane $S_{zz}(p,T)$ over in-plane $S_{xx}(p,T)$ and (d) in-plane $S_{xx}(n,T)$ at different temperatures. The temperature ranges from 100 K to 700 K for some practical reasons. Hole and electron dopings are respectively used in panels (a)–(c) and panel (d). Experimental data with $p = 7.6 \times 10^{16}$ and 1.0×10^{17} cm^{-3} at 200 K obtained by Mansfield and Salam[17], are respectively marked by filled triangles and squares in panel (b). The p and n as the x axis represent the concentrations of the doped hole and electron, respectively.

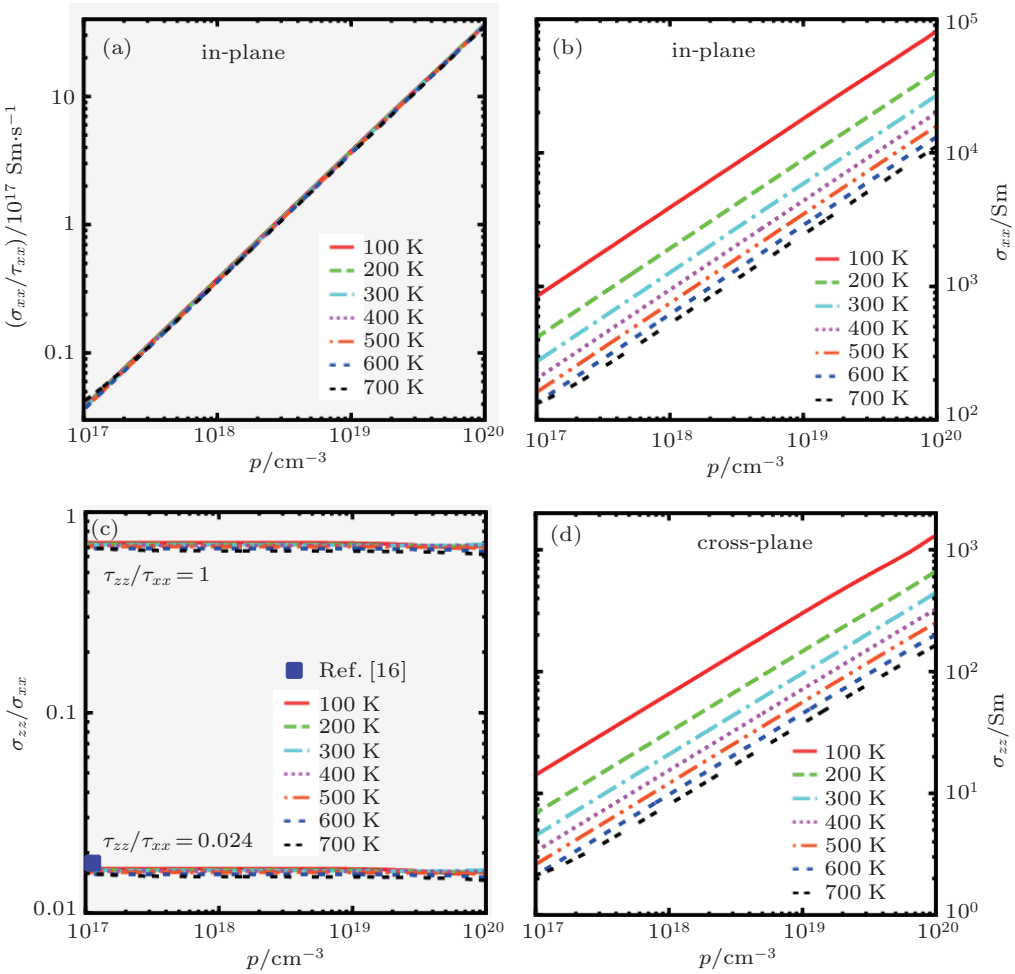


Fig. 3. (color online) Doping level dependences of (a) in-plane σ_{xx}/τ_{xx}, (b) in-plane electrical conductivity σ_{xx}, (c) ratio of cross-plane σ_{zz}/τ_{zz} over in-plane σ_{xx}/τ_{xx} and (d) cross-plane σ_{zz} at different temperatures. Isotropic electronic scattering time and anisotropic electronic scattering time are respectively assumed in panel (c), for instance, $\tau_{zz}/\tau_{xx} = 1$ and 0.024, the anisotropic one fits well the experimental data in the blue square from Thakurta *et al.*[16] and thereby is used to derive σ_{zz} in panel (d).

Based on the energy-independent scattering time approximation, it is quite straightforward to obtain the doping dependences of σ/τ at various temperatures from the electronic band structure, upon which we can calculate σ if τ is known. In Fig. 3(a), we show calculated σ_{xx}/τ_{xx} depending on the hole doping and temperature. We find an almost temperature independent σ_{xx}/τ_{xx} with an approximately linear dependence on doping, namely, $\sigma_{xx}/\tau_{xx} \sim T^0 p$. For a quadratic band dispersion in the electron-phonon approximation, $\sigma \sim p^{2/3}T^{-1}$ stands, this results in $\tau_{xx} \sim T^{-1}p^{-1/3}$, which is inconsistent with the analytical treatment of carriers scattered by lattice vibrations in a semiconductor.[6,41] To calculate σ_{xx}, we need some experimental inputs to obtain $\tau_{xx}(T,p)$. Here, we use $\sigma_{xx} = 0.16\ \Omega^{-1}\cdot\text{cm}^{-1}$ at 100 K and doping 1.4×10^{15} cm^{-3} from the experimental data by Thakurta *et al.*[16] and obtain $\tau_{xx} = 3.04\times10^{-6}T^{-1}p^{-1/3}$, where T and p are in units of K and cm^{-3}, respectively. Plugging it into our calculated σ/τ, we show $\sigma_{xx}(T,p)$ in Fig. 3(b) and power factor $\sigma_{xx}S^2_{xx}(T,p)$ in Fig. 4(a).

The electrical conductivity along the c axis is also calculated; a strong anisotropy is found between the in-plane and cross-plane carrier scattering time. When isotropic carrier scattering time τ is assumed, namely, $\tau_{zz}/\tau_{xx} = 1$, we obtain σ_{zz}/σ_{xx} close to unity in Fig. 3(c), which is against the reported result.[16] To fit σ_{xx}/σ_{zz} of two orders of magnitude in experiment, we use $\tau_{zz}/\tau_{xx} = 0.024$, which suggests that a strong anisotropy of carrier scattering time should play a role in this system. Using $\tau_{zz} = 7.30\times10^{-8}T^{-1}p^{-1/3}$, we are able to calculate $\sigma_{zz}(T,p)$ and show it in Fig. 3(d). Clearly, doping can substantially improve the electrical conductivity but a difference of two orders of magnitude always exists between σ_{zz} and σ_{xx}.

With the thermopower and the electrical conductivity available, we are able to evaluate the power factor. For an optimized thermoelectric performance, the corresponding doping level and temperature to the peak values of the power factor are more concerned here. Both power factors along two perpendicular directions have peak values spanning in a wide doping range from 10^{17} cm^{-3} to 10^{20} cm^{-3}. From Fig. 4, the value of the peak power factor is nearly constant, while its temperature increases with the increasing hole doping level. Due to the anisotropic carrier scattering time τ, a nearly 50-fold dif-

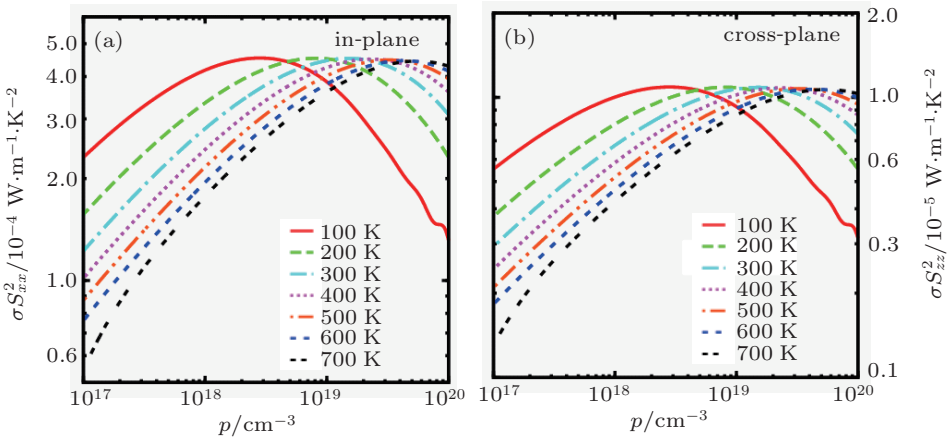


Fig. 4. (color online) Doping level dependences of (a) $\sigma_{xx}S_{xx}^2$ and (b) $\sigma_{zz}S_{zz}^2$ of p-type MoS_2 at different temperatures.

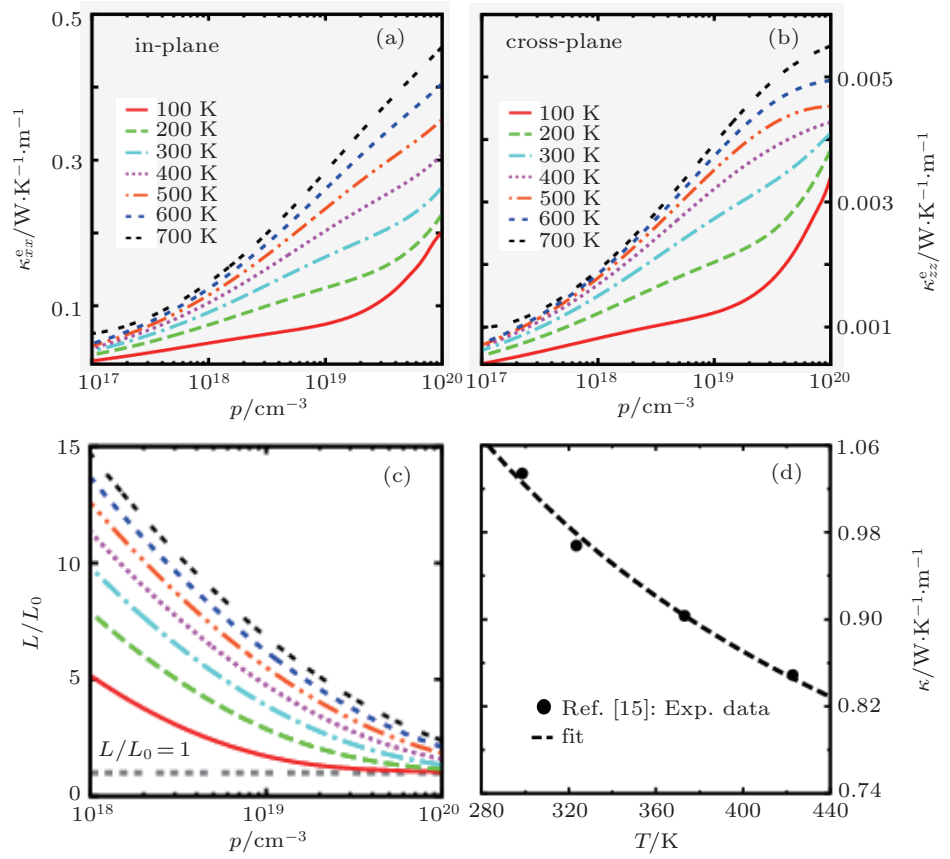


Fig. 5. (color online) (a) In-plane electronic thermal conductivity κ_{xx}^{e}, (b) cross-plane κ_{zz}^{e} and (c) in-plane L/L_0, each as a function of doping and temperature, here $L = \kappa/(\sigma T)$ and L_0 is the Lorenz number 2.44×10^{-8} W·Ω·K^{-2}. (d) Temperature dependence of thermal conductivity κ_{zz} from experiment by Kim *et al.*,[15] the data are presented by filled circles and fitted by $\kappa = 183.103/T + 0.412671$ in the dashed line. Meanwhile, κ_{xx} is taken to be four times as big as κ_{zz}.[42]

ference is found between the in-plane and cross-plane power factors, e.g., σS_{xx}^2 and σS_{zz}^2 maxima at 700 K are respectively 4.1×10^{-4} W/m/K^2 and 1.0×10^{-5} W/m/K^2. The in-plane PF is close to that of good thermoelectric materials.[34]

To optimize the ZT value, it is also essential to know thermal conductivity κ, including electronic thermal conductivity κ_{e} and lattice thermal conductivity κ_{l}. Based on the scattering time approximation previously discussed, we firstly calculate the electronic thermal conductivity and show it in Figs. 5(a) and 5(b). The κ_{e} increases with increasing carrier density p and temperature. A difference of at least two orders of magnitude between κ_{xx}^{e} and κ_{zz}^{e} is found, which is consistent with the electrical conductivity case. Usually one obtains κ_{e} from electrical conductivity σ by using the Wiedemann–Franz law, namely, $\kappa_{\mathrm{e}}/(\sigma T) = 2.44\times10^{-8}$ W·Ω·K^{-2}, the so-called Lorenz number. However, it seems not to be the case here. In Fig. 5(c), we normalize L $(= \kappa_{\mathrm{e}}/(\sigma T))$ by the Lorenz number and plot it as a function of doping and temperature. The L/L_0 is close to one as the carrier density goes beyond 10^{20} cm^{-3}. Unlike the electronic thermal conductivity κ_{e}, the

lattice thermal conductivity κ_l cannot be calculated from the electronic band structure. Here, we use the experimental data from Ref. [15] and show it in Fig. 5(d). Kim *et al.*[15] measured the temperature dependence of κ_{zz} for an MoS_2 sample, as shown by the filled circles in Fig. 5(d). The lattice thermal conductivity dominates in the cross-plane direction, with two orders of magnitude bigger than κ_{zz}^e. While the in-plane κ_l, taken to be four times as big as the cross-plane one[42], is comparable to κ_e. We fit the experimental data by using $\kappa_{zz} = 183.103/T + 0.412671$. It seems that the Umklapp process, which usually has $\kappa \sim 1/T$, shows up and the thermal conductivity gets softened with the increasing temperature.

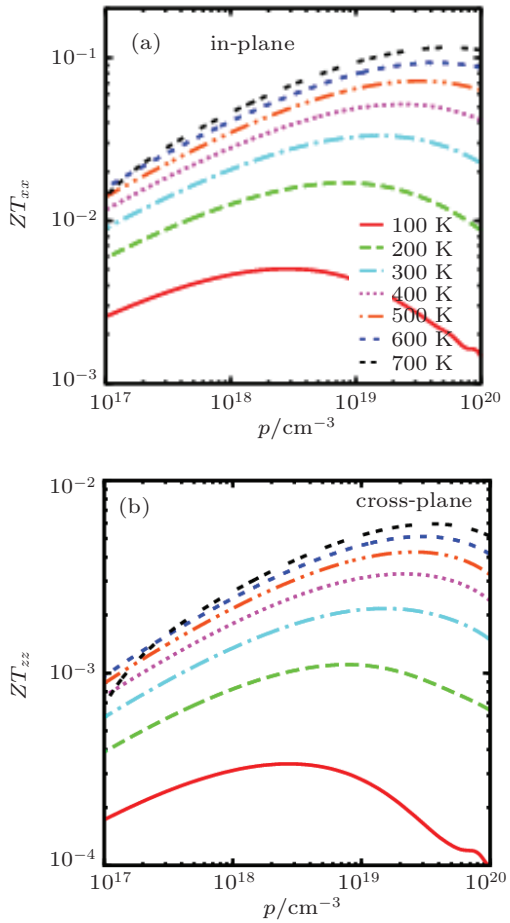


Fig. 6. (color online) Doping level dependent (a) in-plane and (b) cross-plane figure of merit coefficients of p-type MoS_2 at different temperatures. The experimental thermal conductivities κ in Fig. 5(d) are used.

All the data obtained above allow us to calculate ZT as a function of temperature and hole doping along two directions, which is shown in Figs. 6(a) and 6(b). The optimum ZT value increases with increasing temperature, so does the corresponding optimum doping level. In-plane is better than cross-plane for thermoelectric conversion, with its ZT up to 0.10 and saturated around 700 K, as shown in Fig. 6. This value is close to what is obtained by applying a high pressure on MoS_2.[19] We may further reduce κ by random stacking according to Kim[15] and Chiritescu *et al.*,[14] but its effect on the electrical transport needs to be checked as it may compromise the gain of ZT by reducing the thermal conductivity. The high pressure leads to a preference of cross-plane over in-plane, while doping gives rise to an opposite trend. We note that experimental doping in transition metal chalcogenides[43] can be obtainable up to 10^{22} cm^{-3}.

4. Conclusion

By combining *ab initio* band structure calculation with the semi-classical Boltzmann transport theory, we theoretically studied the doping and temperature dependences of thermoelectric transport properties of 2H-MoS_2. Anisotropic electronic scattering time has to be considered to account for the difference between in-plane and cross-plane electrical conductivities σ, which also gives rise to an anisotropy in electronic thermal conductivity κ_e. In-plane thermal conductivity κ_e^{xx} is not negligible compared to lattice thermal conductivity κ_l^{xx}, while cross-plane lattice thermal conductivity κ_l^{zz} dominates over lattice thermal conductivity κ_e^{zz}. In contrast to the anisotropy of σ and κ_e, thermopower, which is attainable more than 200 μV/K over a wide range of doping and temperature, shows a vanishing anisotropy for doping over 10^{17} cm^{-3}, which likely arises from the decoupling of two perpendicular conduction channels. The maximum ZT can reach 0.1 at around 700 K with a carrier density of 10^{20} cm^{-3}, which may go higher if a restacking process is used to further reduce the thermal conductivity. A preference for the in-plane thermoelectric transport by doping is demonstrated.

References

[1] Rapoport L, Bilik Y, Feldman Y, Homyonfer M, Cohen S R and Tenne R 1997 *Nature* **387** 791
[2] Martin J M, Donnet C and Mogne T L 1993 *Phys. Rev. B* **48** 10583
[3] Gates B C 1992 *Catalytic Chemistry* (New York: Wiley) p. 1
[4] Zong X, Yan H J, Wu G P, Ma G J, Wen F Y, Wang L and Li C 2008 *J. Am. Chem. Soc.* **130** 7176
[5] McGovern I T, Dietz E, Rotermund H H, Bradshaw A M, Braun W, Radlik W and McGilp J F 1985 *Surf. Sci.* **152–153** 1203
[6] Radisavljevic B, Radenovic A, Brivio J, Giacometti V and Kis A 2011 *Nature Nanotechnol.* **6** 147
[7] Li Y B, Bando Y and Golberg D 2003 *Appl. Phys. Lett.* **82** 1962
[8] Gourmelon E, Lignierb O, Hadoudaa H, Couturierb G, Bern'edea J C, Teddb J, Pouzeta J and Salardenneb J 1997 *Sol. Energy Mater. Sol. Cells* **46** 115
[9] Chen J, Kuriyama N, Yuan H T, Takeshita H T and Sakai T 2001 *J. Am. Chem. Soc.* **123** 11813
[10] Xiao J, Choi D, Cosimbescu L, Koech P, Liu J and Lemmon J P 2010 *Chem. Mater.* **22** 4522
[11] Mak K F, Lee C G, Hone J, Shan J and Heinz T F 2010 *Phys. Rev. Lett.* **105** 136805
[12] Lee C G, Yan H G, Brus L E, Heinz T F, Hone J and Ryu S 2011 *ACS Nano* **4** 2695
[13] Ataca C, Topsakal M, Aktürk E and Ciraci S 2011 *J. Phys. Chem. C* **115** 16354
[14] Chiritescu C, Cahill D G, Nguyen N, Johnson D, Bodapati A, Keblinski P and Zschack P 2007 *Science* **315** 351
[15] Kim J Y, Choi S M, Seo W S and Cho W S 2010 *Bull. Korean Chem. Soc.* **31** 3225

[16] Thakurta S R G and Dutta A K 1983 *J. Phys. Chem. Solids* **44** 407
[17] Mansfield R and Salam S A 1953 *Proc. Phys. Soc. B* **66** 377
[18] Agarwal M K and Talele L T 1986 *Sol. State Comm.* **59** 549
[19] Guo H H, Yang T, Tao P, Wang Y and Zhang Z D 2013 *J. Appl. Phys.* **113** 013709
[20] Mahan G D 1998 *Solid State Physics* **Vol. 51** (Ehrenreich H and Saepen F, ed.) (San Diego: Academic Press) pp. 82–152
[21] Hu H, Cai J M, Zhang C D, Gao M, Pan Y, Du S X, Sun Q F, Niu Q, Xie X C and Gao H J 2010 *Chin. Phys. B* **19** 037202
[22] Sun Y, Wang C L, Wang H C, Su W B, Liu J, Peng H and Mei L M 2011 *Acta Phys. Sin.* **60** 087204 (in Chinese)
[23] Li P C, Yang H S, Li Z Q, Chai Y S and Cao L Z 2002 *Chin. Phys.* **11** 282
[24] Wang H C, Wang C L, Su W B, Liu J, Sun Y, Peng H, Zhang J L, Zhao M L, Li J C, Yin N and Mei L M 2009 *Chin. Phys. Lett.* **26** 107301
[25] Blaha P, Schwarz K, Madsen G, Kvasnicka D and Luitz J 2011 *WIEN2k: An augmented plane wave plus local orbitals program for calculating crystal properties* (TU Vienna, Vienna)
[26] Perdew J P, Burke K and Ernzerhof M 1996 *Phys. Rev. Lett.* **77** 3865
[27] Engel E and Vosko S H 1993 *Phys. Rev. B* **47** 13164
[28] Coehoorn R, Haas C, Dijkstra J and Flipse C J F 1987 *Phys. Rev. B* **35** 6195
[29] Madsen G K H, Schwarz K, Blaha P and Singh D J 2003 *Phys. Rev. B* **68** 125212
[30] Wu Y D, He Y J and Wang Z M 2004 *Chin. Phys.* **21** 1848
[31] Parker D, Du M H and Singh D J 2011 *Phys. Rev. B* **83** 245111
[32] Zhang L and Singh D J 2009 *Phys. Rev. B* **80** 075117
[33] Han S W, Kwon H, Kim S K, Ryu S, Yun W S, Kim D H, Hwang J H, Kang J S, Baik J, Shin H J and Hong S C 2011 *Phys. Rev. B* **84** 045409
[34] Kam K K and Parkinson B A 1982 *J. Phys. Chem.* **86** 463
[35] Rowe D M and Min G 1995 *J. Mater. Sci. Lett.* **14** 617
[36] Zhang Y, Ke X Z, Chen C F, Yang J H and Kent P R C 2011 *Phys. Rev. Lett.* **106** 206601
[37] Snyder G J and Toberer E S 2008 *Nature Mater.* **7** 105
[38] Ong K P, Singh D J and Wu P 2010 *Phys. Rev. Lett.* **104** 176601
[39] Ong K P, Zhang J, Tse J S and Wu P 2010 *Phys. Rev. B* **81** 115120
[40] Tang G D, Guo H H, Yang T, Zhang D W, Xu X N, Wang L Y, Wang Z H, Wen H H, Zhang Z D and Du Y W 2011 *Appl. Phys. Lett.* **98** 202109
[41] Ziman J M 1972 *Principles of the Theory of Solids* (2nd edn.) (Cambridge: Cambridge University Press) p. 228
[42] Varshneya V, Patnaikc S S, Muratorea C, Roya A K, Voevodina A A and Farmera B L 2010 *Computational Materials Science* **48** 101
[43] Miyazaki Y, Ogawa H and Kajitani T 2004 *Jpn. J. Appl. Phys.* **43** L1202